

Predictions of the Poses and Affinity of a Ligand over the Entire Surface of a NEET Protein: The Case of Human MitoNEET

Ke Zuo, Riccardo Capelli, Giulia Rossetti, Rachel Nechushtai, and Paolo Carloni*



Cite This: *J. Chem. Inf. Model.* 2023, 63, 643–654



Read Online

ACCESS |



Metrics & More

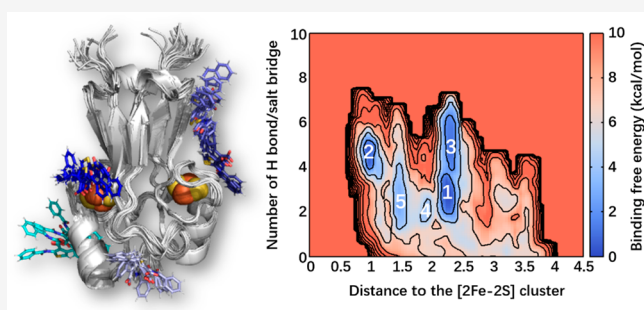


Article Recommendations



Supporting Information

ABSTRACT: Human NEET proteins contain two [2Fe–2S] iron–sulfur clusters, bound to three Cys residues and one His residue. They exist in two redox states. Recently, these proteins have revealed themselves as attractive drug targets for mitochondrial dysfunction-related diseases, such as type 2 diabetes, Wolfram syndrome 2, and cancers. Unfortunately, the lack of information and mechanistic understanding of ligands binding to the whole functional, cytoplasmatic domain has limited rational drug design approaches. Here, we use an enhanced sampling technique, volume-based metadynamics, recently developed by a team involving some of us, to predict the poses and affinity of the 2-benzamido-4-(1,2,3,4-tetrahydronaphthalen-2-yl)-thiophene-3-carboxylate ligand to the entire surface of the cytoplasmatic domain of the human NEET protein mitoNEET (mNT) in an aqueous solution. The calculations, based on the recently published X-ray structure of the complex, are consistent with the measured affinity. The calculated free energy landscape revealed that the ligand can bind in multiple sites and with poses other than the one found in the X-ray. This difference is likely to be caused by crystal packing effects that allow the ligand to interact with multiple adjacent NEET protein copies. Such extra contacts are of course absent in the solution; therefore, the X-ray pose is only transient in our calculations, where the binding free energy correlates with the number of contacts. We further evaluated how the reduction and protonation of the Fe-bound histidine, as well as temperature, can affect ligand binding. Both such modifications introduce the possibility for the ligand to bind in an area of the protein other than the one observed in the X-ray, with no or little impact on affinity. Overall, our study can provide insights on the molecular recognition mechanisms of ligand binding to mNT in different oxidative conditions, possibly helping rational drug design of NEET ligands.



1. INTRODUCTION

The human NEET iron–sulfur proteins (mNT, NAF-1, MiNT)^{1–3} play a key role in mitochondrial dysfunction associated with diseases, such as metabolic diseases, cancers, and progressive neurodegenerative diseases.^{4,5} While MiNT is a monomeric protein located inside the mitochondria,⁴ the other two are homodimers localized on the outer membrane of the mitochondria with a transmembrane domain and a cytosolic domain. Each subunit features a two iron-two sulfur cluster coordinated by three cysteines and one histidine. The histidine-bound iron is closer to the protein surface, which can exist as an Fe(II) or an Fe(III) ion, while the other metal (an Fe(III) ion) is buried in the protein (Chart S1 in the SI). The reduced cluster is kinetically inert,^{6,7} and it can be released/transferred to apo-acceptor(s)⁴ (and increasingly so by lowering the pH) upon oxidation. The aberrant cluster in disease conditions release can lead to cell derangement.

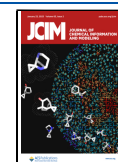
Recently, these proteins have emerged as attractive targets for pharmacological intervention. Indeed, small molecules binding to these proteins^{5,8–10} have been shown to modulate the kinetics of cluster release. For instance, compound **A** in Figure 1 accelerates the [2Fe–2S] clusters of mNT and NAF-1

release to apo-acceptors *in vitro*, while furosemide does the opposite (Figure 1).⁹ Hence, in principle, specific ligands could be used to restore the normal functioning of these proteins.

The first pose of a ligand predicted by molecular simulation is that of furosemide to oxidized mNT in an aqueous solution. Tailored enhanced sampling simulations,¹² performed by some of us, were consistent with the measured binding affinities.⁹ Interestingly, they suggested not only the binding pose close to the [2Fe–2S] cluster determined by X-ray studies^{9,12} but also an ensemble of poses around the cluster itself. The difference was ascribed to crystal packing effects, which contribute to stabilizing a single specific ligand pose in the experimental structure.¹² These predictions were carried out by imposing the binding in the [2Fe–2S] cluster region.^{9,12} Here, we

Received: October 14, 2022

Published: January 9, 2023



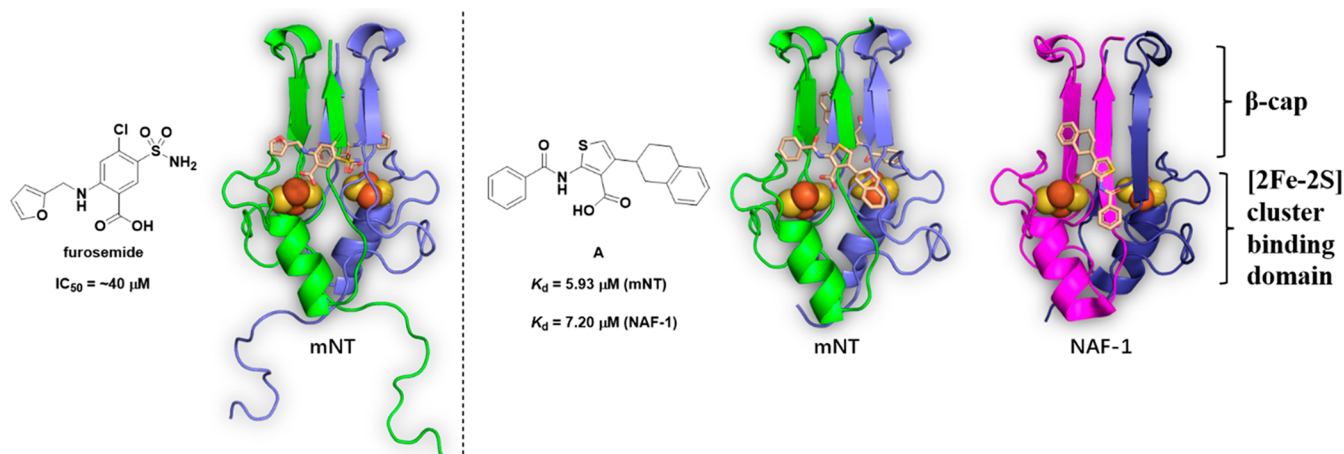


Figure 1. Chemical structure, binding affinity, and crystal structures of 2-benzamido-4-(1,2,3,4-tetrahydronaphthalen-2-yl)-thiophene-3-carboxylate ("A") and of furosemide with mNT^{9,11} (PDB IDs: 6DE9,⁹ 7P0O,¹¹ and 7P0P¹¹ for the furosemide-mNT, A-mNT, and A-NAF-1 complexes, respectively). The ligands (represented as wheat sticks) bind to the [2Fe-2S] cluster (represented as spheres) regions. mNT is shown in green/slate and magenta/deep blue cartoons, respectively. The ligand poses in the X-ray structure are similar.^{9,11}

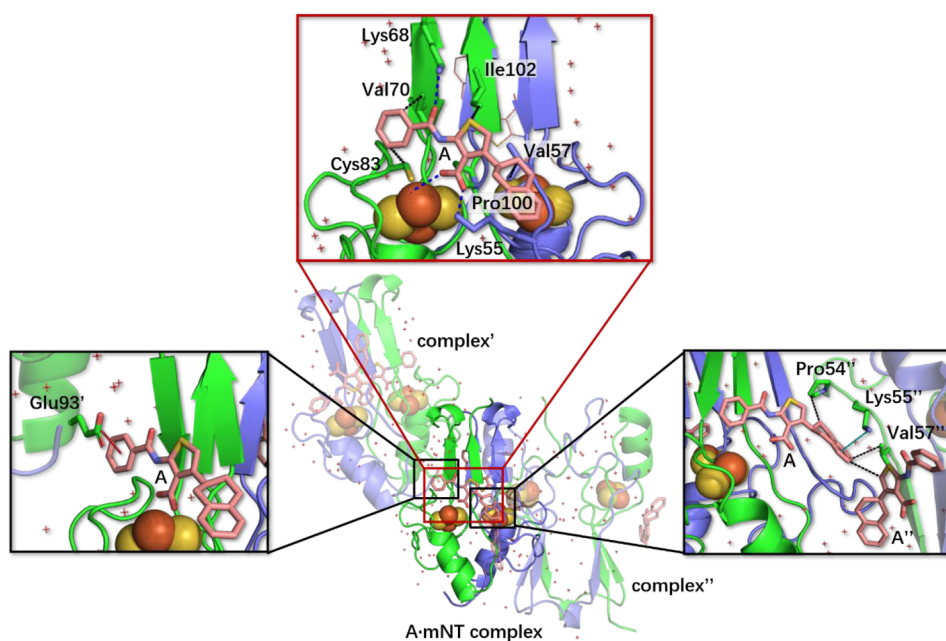


Figure 2. Ligand/protein interactions in the X-ray structure of the A-mNT complex. A's amide oxygen forms an H-bond with Lys68, its carboxylate group forms a salt bridge with Lys55 and a water molecule (blue dashes, top panel), its phenyl ring forms a hydrophobic interaction with Val70 and Cys83, its thiophene moiety forms an interaction with Pro100 and Ile102, and its tetralin group forms an interaction with Val57 (black dashes, top panel). The binding pose is further stabilized by the interactions with two adjacent A-mNT complexes. It forms a π -anion interaction between its phenyl ring and Glu93' (red dashes, left panel) and a π -cation interaction with Lys55'' (cyan dashes) via its tetralin ring, as well as hydrophobic interactions with Pro54'', Val57'', and A'' in complex'' (black dashes, right panel). A is displayed as a wheat stick model, and mNT is shown with a green/slate cartoon.

address the question of whether a ligand can also bind outside the cluster binding domain. We focus on the binding of 2-benzamido-4-(1,2,3,4-tetrahydronaphthalen-2-yl)-thiophene-3-carboxylate (A hereafter) to mNT, for which both affinity and experimental structural information are available.¹¹ The X-ray structure of the A-mNT complex shows that A interacts also with two adjacent A-mNT complexes in the crystal (Figure 2). Specifically, A's phenyl forms π -anion interactions¹³ with Glu93' from another mNT protein in the crystal, and A's tetralin forms π -cation interactions¹⁴ with Lys55'' from a second mNT protein, as well as hydrophobic interactions with

Pro54'' and Val57'' and with the ligand A'' bound to the second protein (Figure 2). Therefore, such crystal contact might have favored this binding pose over other possible ones. Such overstabilization is of course not present in an *in cell* environment, opening the possibility of other binding poses and binding sites for A.

Here, we explore binding to the entire surface of the protein (that is, including regions other than that of the cluster). Namely, we predict the free energy landscape associated with poses all over the surface of the protein by using volume-based metadynamics, developed in a team involving some of us.¹⁵ We

Table 1. Simulated Systems in This Study^a

name	Fe-bound histidine	redox state	charge of the protein (e)	number of Na ⁺ ions	number of Cl ⁻ ions	number of H ₂ O molecules
I	imidazolate	oxidized	-2	54	51	28,562
II	imidazole	oxidized	0	54	53	28,561
III	imidazolate	reduced	-4	54	49	28,564
IV	imidazole	reduced	-2	54	51	28,563

^aHere, we consider four complexes (I–IV) of the A-mNT complex. They differ from the oxidation state and N_ε@His87 protonation state for both clusters. Some of the details of the simulation setup are also included.

perform our protocol for both redox states of the [2Fe–2S] clusters and protonation states of the Fe-bound His87 (Table 1). Anticipating our results, we find that the ligand can indeed bind in several binding poses and a binding site other than the X-ray one. Because the free energy of binding turns out to correlate with the number of contacts between the ligand and the protein, the crystallographic pose is only transient in our simulations since there are no contacts with adjacent complexes in the crystals, like observed in the X-ray, that can stabilize such a pose.

2. METHODS

2.1. Ligand Preparation. A was constructed using ChemBio3D Ultra 12.0. It was energy-minimized first to the minimal root mean squared (RMS) gradient of 0.01 kcal·mol⁻¹·Å⁻¹, based on the MM2 force field,¹⁶ using Chem3D 16.0, then to the maximum and RMS force on the nuclei which are less than 0.00045 hartree/Bohr and 0.00035 hartree/Bohr, respectively, and then to the maximum and RMS nuclei displacement which are less than 0.0018 and 0.0012 Å, respectively, at the HF/6-31G(d)^{17,18} level of theory, employing the Gaussian 09 software package.¹⁹

2.2. Molecular Docking. We generated an educated starting structure of the ligand close to the [2Fe–2S] cluster by docking the ligand A on the oxidized human mNT cytosolic domain in the free state (PDB ID: 2QH7).¹ This procedure does not bias the molecular dynamics simulations toward the pose of the X-ray structure of the complex.¹ The latter hardly differs from that in complex with the ligand (RMSD between the two backbones is 0.14 Å, and that of the ligand binding region in the X-ray structure is equal to 0.11 Å, see Chart S2 in the SI.). First, we performed restrained energy minimization on mNT using the OPLS 2005 force field.^{20,21} Then, the program Glide^{22,23} was used, with one equivalent of ligand for an equivalent of protein, consistently with the binding essays performed in ref 11. [It differs from the conditions of the X-ray structure where the ligand to protein stoichiometric ratio is 2 to 111.] The convergence criterion for RMS fluctuation of heavy atoms was set to less than 0.3 Å. We docked the ligand pose in the proximity of the [2Fe–2S] cluster binding region. For complexes I and II (Table 1), we assigned the charge +3 to both metal ions. For the other two redox states, we set the charges to +3 to the iron buried inside the protein and +2 to the His ligated iron. As the docking program does not consider His residues in their deprotonated states, we kept the same protonation of His87 across I–IV. We used a cubic grid of 20 Å edges, with a spacing of 1.0 Å. We set the remaining docking parameters to the default values (see Table S1 in the SI). The docking score function is the GlideScore function.²² The top ranked structure was selected for MD calculations.

2.3. MD Simulation. The I–IV complexes were embedded in a dodecahedron filled with water, with a minimum distance of 30 Å from the protein to the box edge. Na⁺ and Cl⁻ ions

were added to neutralize the system and to mimic the ionic strength of ~0.1 mM used in the *in vitro* experiments of ligand binding and crystallization.¹¹ The overall systems were set to neutral (Table 1). Periodic boundary conditions were applied.

The force fields for the mNT protein, water, and counterions were those used in refs 7 and 24, *i.e.*, the AMBER force-field 99SB-ILDN,^{25,26} TIP3P,²⁷ and Åqvist potentials,²⁸ respectively. The force field of A was the GAFF²⁹ with semiempirical AM1-BCC partial charges³⁰ (see Tables S2 and S3 in the SI).

Long range electrostatic interactions were calculated using particle mesh Ewald (PME).³¹ The cutoff for short-range electrostatics and for van der Waals interactions was set to 14 Å. We constrained all the chemical bonds by using the LINCS algorithm.³² The Nosé–Hoover thermostat^{33,34} and Parrinello–Rahman barostat³⁵ were used to keep constant temperature (293 or 310 K) and pressure (1.0 bar), respectively. The time constants for temperature and pressure coupling were 0.4 and 0.8 ps, respectively. The time integration step was set to 2 fs.

All the systems were energy-minimized by 50,000-step steepest descent and 50,000-step conjugate gradient algorithms. Then, they underwent heating by 300 K in 1 ns simulated annealing, followed by 50 ns NVT MD and 50 ns NPT MD equilibration phases. Finally, 500 ns production trajectories were collected at 310 K and 1 bar for mNT (I–IV) and one trajectory of mNT (I) at 293 K. All the calculations were carried out with GROMACS 2019.2.^{36,37} The last snapshot of the 500 ns-long MD simulations of the complexes in Table 1 was used as starting structures.

2.4. Volume-Based Metadynamics. The free energy associated with the A binding/unbinding process was calculated via the volume-based well-tempered metadynamics method.¹⁵ The approach can be seen as a multipathway extension of funnel well-tempered metadynamics,³⁸ where a funnel-shaped potential limits the volume accessible to the ligand in the solvated space, considering a single egress pathway for the ligand. Here, the chosen collective variables (CVs) are represented by the spherical coordinates of a ligand in the reference frame of the host protein (*i.e.*, radial distance ρ , azimuthal angle θ , and polar angle φ). To limit the sampling of the conformational space to the relevant configurations for the binding/unbinding process and to favor recrossing events, the accessible volume of the ligand is limited to a sphere of radius ρ_s centered in the center of mass of mNT. A repulsive potential $U\{\rho(t)\}$ is then added at the border of the sphere

$$U[\rho(t)] = \begin{cases} \frac{1}{2}k[\rho(t) - \rho_s], & \text{if } \rho(t) > \rho_s \\ 0, & \text{else} \end{cases} \quad (1)$$

where k should be large enough to prevent the ligand from escaping the confining volume (in this work, it is 10,000 kJ·mol⁻¹·nm⁻¹ as in ref 15), $\rho(t)$ is the distance of the ligand from

the center of mass of mNT at a given time t , and ρ_s was set to 30 Å.

The application of the restraining potential $U\{\rho(t)\}$ causes a modification of the translational entropy of the system.^{39,40} To remove such contribution from the binding free energy ΔG_b^0 , we can add a correction term

$$\Delta G_b^0 = \Delta G_{\text{Metad}} - T\Delta S \quad (2)$$

$$-T\Delta S = RT \ln \left(\frac{V^0}{\frac{4}{3}\pi\rho_s^3 - V_{\text{prot}}} \right) \quad (3)$$

where R is the gas constant, T is the system temperature, the standard volume V^0 is equal to 1,660 Å³, ΔG_{Metad} is the binding free energy obtained by metadynamics simulation, and V_{prot} is the volume of the NEET proteins (44,200 Å³ for mNT).

The widths of Gaussians were chosen to be 0.1 nm, $\pi/16$ rad, and $\pi/8$ rad for ρ , θ , and φ , respectively, following the protocol of ref 15. The height of the Gaussian was set to 1.2 kJ·mol⁻¹, and the bias factor was set to 20, with a deposition rate of 1 ps⁻¹. The temperature and pressure were maintained with the same thermostat and barostat described in the initial equilibration (section 2.3). Five 300 ns volume-based well-tempered metadynamics simulations were carried out: I at 293 K and I–IV at 310 K. We used PLUMED-2.6.0^{41,42} patched with GROMACS 2019.2.^{36,37}

We projected the free energy landscape onto the two following CVs: (i) the distance from the ligand center to the center of the [2Fe–2S] cluster and (ii) the number of hydrogen bonds (H-bonds) and salt bridges defined by eq 4

$$n = \sum_j \frac{1 - (r_{ij}/r_0)^a}{1 - (r_{ij}/r_0)^b} \quad (4)$$

where a and b are set to 8 and 12, respectively, $r_0 = 2.5$ Å,⁴³ and atoms i and j represent the donor and acceptor atoms, respectively. The coordination numbers between A (set of atoms i) and protein (set of atoms j) were defined also by using eq 4, with $r_0 = 4.5$ Å, and a and b are 6 and 12, respectively.¹⁵

3. RESULTS AND DISCUSSION

We consider here four complexes (I–IV, see Table 1) of the A-mNT complex, differing in the oxidation state and N_e@His87

Table 2. Binding Free Energy Associated with the Formation of the I Complex, as Calculated from Volume-Based Metadynamics at 293 K (ΔG_b^0 , kcal/mol)^a

minimum	ΔG_{Metad}	$-T\Delta S$	ΔG_b^0
1	−5.5	−2.2	−7.7 ± 0.8
2	−3.9	−2.2	−6.1 ± 0.8
3	−2.2	−2.2	−4.4 ± 0.8
4	−1.0	−2.2	−3.2 ± 0.8
5	−0.9	−2.2	−3.1 ± 0.8

^aThe experimental value at 283 K¹¹ is −6.9 kcal/mol.

protonation state of the clusters. We first perform 0.5 μs molecular dynamics at constant temperature and pressure to equilibrate complexes I–IV. The systems appear equilibrated, as shown by plots of the RMSD values against simulated time (see the SI, Figure S1). Next, we predict the free energies of binding and unbinding by ~0.3 μs volume-based metadynamics simulations (Figure S3 in the SI). They are calculated as a function of the spherical CVs. However, in the follow-up discussion, we find it more convenient to plot it as a function of distance to the [2Fe–2S] cluster in the proximity of the ligand along with the number of H-bond and salt bridges.

3.1. From the Crystal to the Aqueous Solution. To study the changes on passing from the crystal to the solution, we investigate the free energy landscape associated with A (un)binding in the aqueous solution. [The temperature is set to 293 K, and N_e is considered deprotonated, as expected at pH 8.0.] We simulate the system at the same temperature as that of the X-ray structure (293 K) and consider (i) the Fe-bound histidine deprotonated, as expected at the pH of crystallization (pH 8.0¹¹) and (ii) the oxidized state (I in Table 1) as in the X-ray structure.

Five minima are identified (Table 2 and Figure 3, Table S4 in the SI) in our free-energy simulations. M 1 and 2 feature the lowest binding free energy (−7.7 ± 0.8 kcal/mol and −6.1 ± 0.8 kcal/mol, respectively). These are consistent with the measured affinity (−6.9 kcal/mol¹¹), within the following caveats: (i) A destabilizes the [2Fe–2S] clusters of mNT *in vitro* and accelerates cluster release;¹¹ this phenomenon could affect the measurement. (ii) The temperature at which free energy has been measured (283 K) differs from that used for crystallization and in these simulations (293 K).¹¹ As the cluster release is kinetically controlled,⁷ here temperature difference could introduce energy inaccuracy.

In these two low-energy minima, the ligand binds relatively close to the [2Fe–2S] cluster binding area, but the poses' orientations differ from that of the X-ray structure. Specifically, in pose 1 (and pose 2), the ligand's tetralin moiety forms hydrophobic interactions with Ala69, Val70, Phe82, and Cys83 (with Val70, Cys83, and Pro100) and polar interactions with Lys68 (with Asp84 and Gly85). Its thiophene ring forms hydrophobic interactions with Pro100 (with Val57 and Ile102). The ligand phenyl ring interacts with Thr88 and Lys89 (with Asn53 and Pro54), the amide oxygen forms H-bonds with a water molecule, and the latter interacts with His87 (to Val57) through an H-bond. Besides, the carboxylate group interacts with Asp84 by H-bonding with two water molecules (by forming salt bridges with Lys55 and water molecules) (see Figure 4A and B).

Next poses 1 and 2 (Figure 3) undergo MD simulations to investigate their variability in the absence of any bias. During MD simulations, A could bind to the cluster binding region, especially poses obtained from pose 2, as in the X-ray structure (2' in Figure S5, see details in the SI).

The minimum 3 is ~1.7 kcal/mol higher than minimum 2. Here, A forms hydrophobic interactions with Phe82 and Ala69 on the β-cap (Figure 4C). A's thiophene ring also forms hydrophobic interactions with Val70, while its phenyl ring forms hydrophobic interactions with Val57, Pro100, and Ile102. In addition, it forms polar interactions with Lys55, Lys68, Gly85, and His87. The amide oxygen and carboxylate groups form H-bonds with water in the solution (Figure 4C).

The minima 4 and 5 are farther ~1.2 kcal/mol higher than minimum 3. [The presence of the protein transmembrane domain (absent in the X-ray structure and in our simulations) may significantly affect the free energy landscape of the region around minimum 4, as the ligands bind close to the latter.] Here, A forms hydrophobic interactions with L1 (Figure 3). Specifically, in minimum 4 (and 5), the tetralin group forms hydrophobic interactions with Pro54 (with His48 and Lys78).

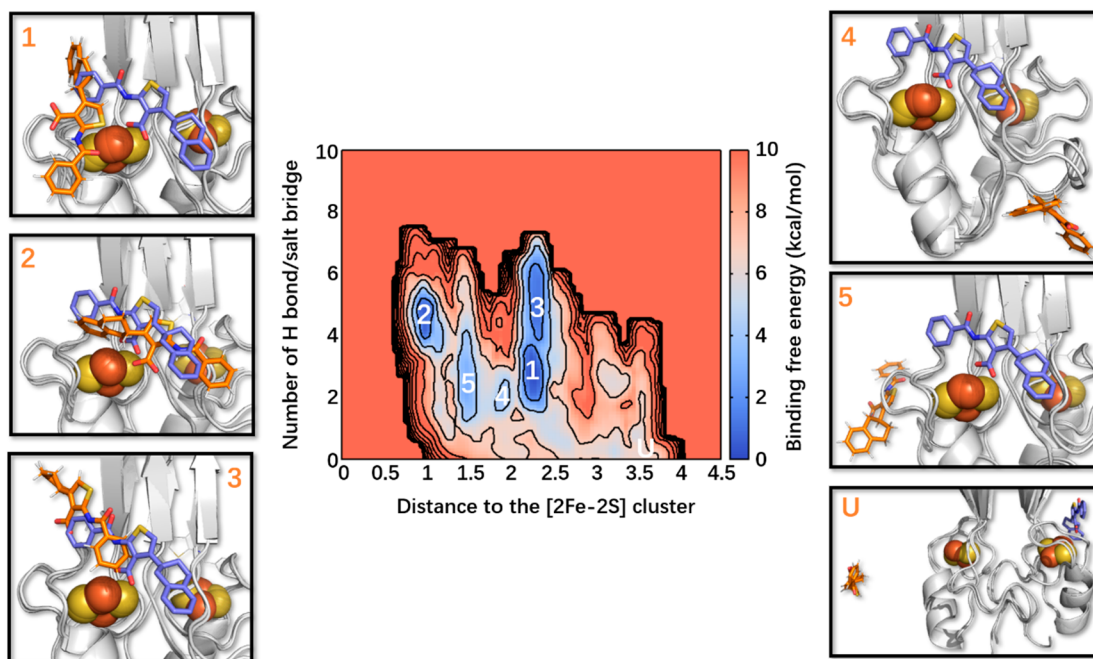


Figure 3. Free energy associated with A binding to mNT (complex I in Table 1) plotted as a function of the distance between the centers of mass of A and of the [2Fe-2S] cluster and the number of H-bonds/salt bridges at 293 K. The crystal binding pose is shown in the slate stick as a reference, while the representative binding poses are shown in orange. 1–5 are the five different binding poses, and U is an unbound state.

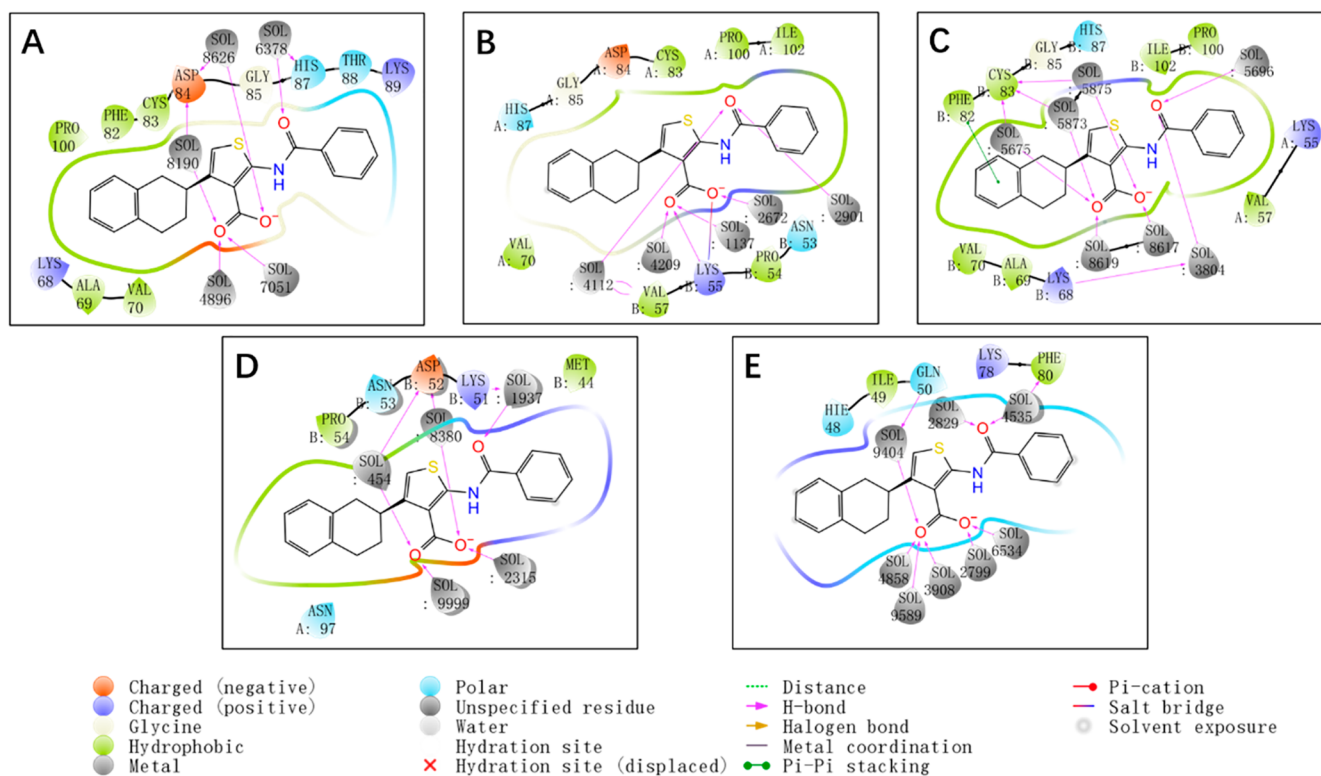


Figure 4. Ligand-protein interaction diagrams of binding poses in Figure 3.

Its thiophene ring interacts with Asn53 and Asn97 (with Ile49 and Phe80), while the phenyl moiety interacts with Met44 (with Gln50). Both amide and carboxylate oxygen form H-bonds with water molecules (Figure 4D and 4E).

As expected, the free energy of binding shows some degrees of correlation with the number of ligand/protein contacts

(c_{protein} , see Methods) across the five poses identified here. This is shown by a plot of the absolute value of the binding free energy ($|\Delta G_b^0|$) against c_{protein} (Figure 5): Poses 4 and 5 in the water solution, which are not significantly populated according to our calculation (see Figure 5A), are associated with the lowest ($|\Delta G_b^0|$) and c_{protein} values. The ligand is highly

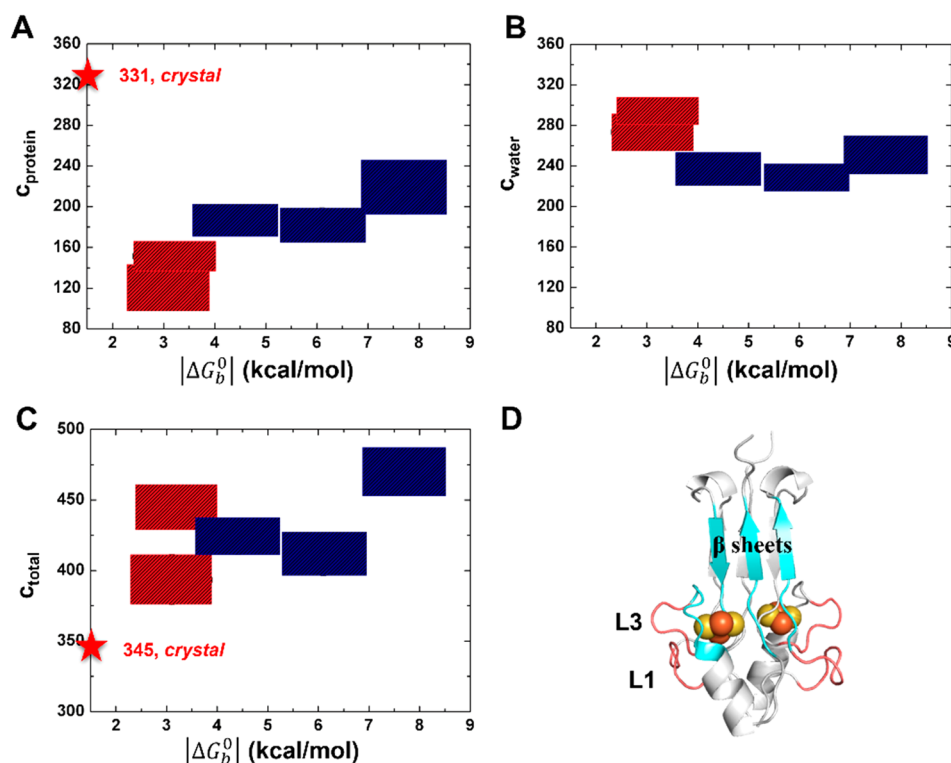


Figure 5. Correlation between the ligand/protein number of contacts and the absolute value of binding free energy ($|\Delta G_b^0|$). Poses 1–3 are shown as the blue squares, and poses 4–5 are shown as the red squares.

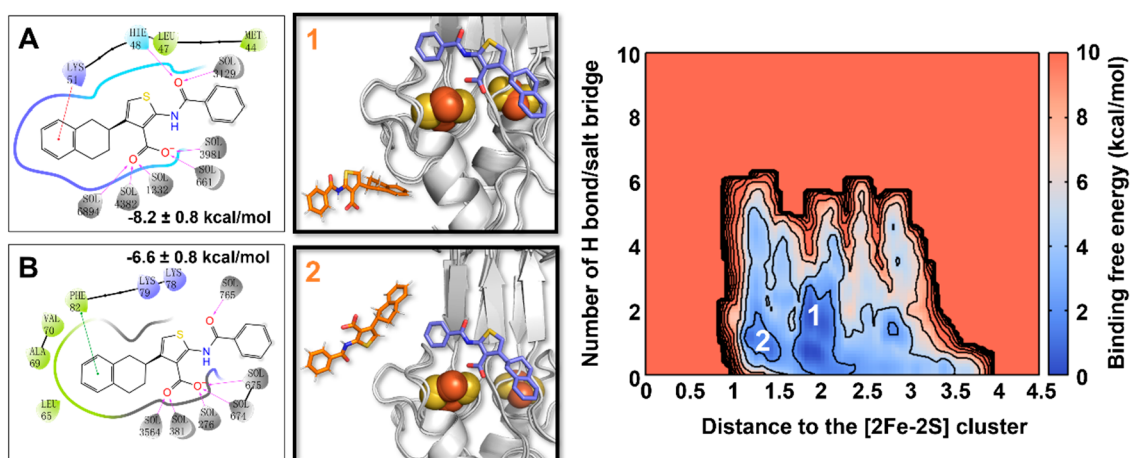


Figure 6. Free energy (kcal/mol) as a function of the distance between the centers of mass of **A** and the [2Fe-2S] cluster and the number of H-bonds/salt bridges at 310 K. The crystal binding pose is shown in the slate stick as a reference, while predicted binding poses are shown in orange.

Table 3. Lowest Binding Free Energy of **A** Bound to mNT at 310 K

complex	lowest binding free energy (kcal/mol)
I	-8.2 ± 0.8
II	-6.2 ± 0.8
III	-8.2 ± 0.8
IV	-7.5 ± 0.8

hydrated, as shown by the high number of contacts of **A** with the solvent (c_{water} , Figure 5B and 5D). Poses 1–3 are associated with higher ($|\Delta G_b^0|$) and c_{protein} values (Figure 5A), and the ligand forms less contacts with water (Figure 5B). Instead, as it might be expected, the total number of contacts

($c_{\text{total}} = c_{\text{protein}} + c_{\text{water}}$) shows no correlation with the free energy (Figure 5C). The number of contacts in the crystal turns out to be far larger than that of any pose in the solution, because of the additional contacts of the complex with its images (Figure 2). Hence, we may expect that the pose in the crystal to be rather different from those in the solution, which is indeed what we find here.

3.2. Binding of the Ligand at 310 K. We evaluate here the impact of temperature on the ligand binding profile. The free energy associated with **A** binding I at physiological temperature, i.e., 310 K, is shown in Figure 6. It differs markedly from that at 293 K. Specifically, only 2 minima are present (out of the 5 minima found at 293 K), and the deepest one has the highest free energy with respect to all the minima

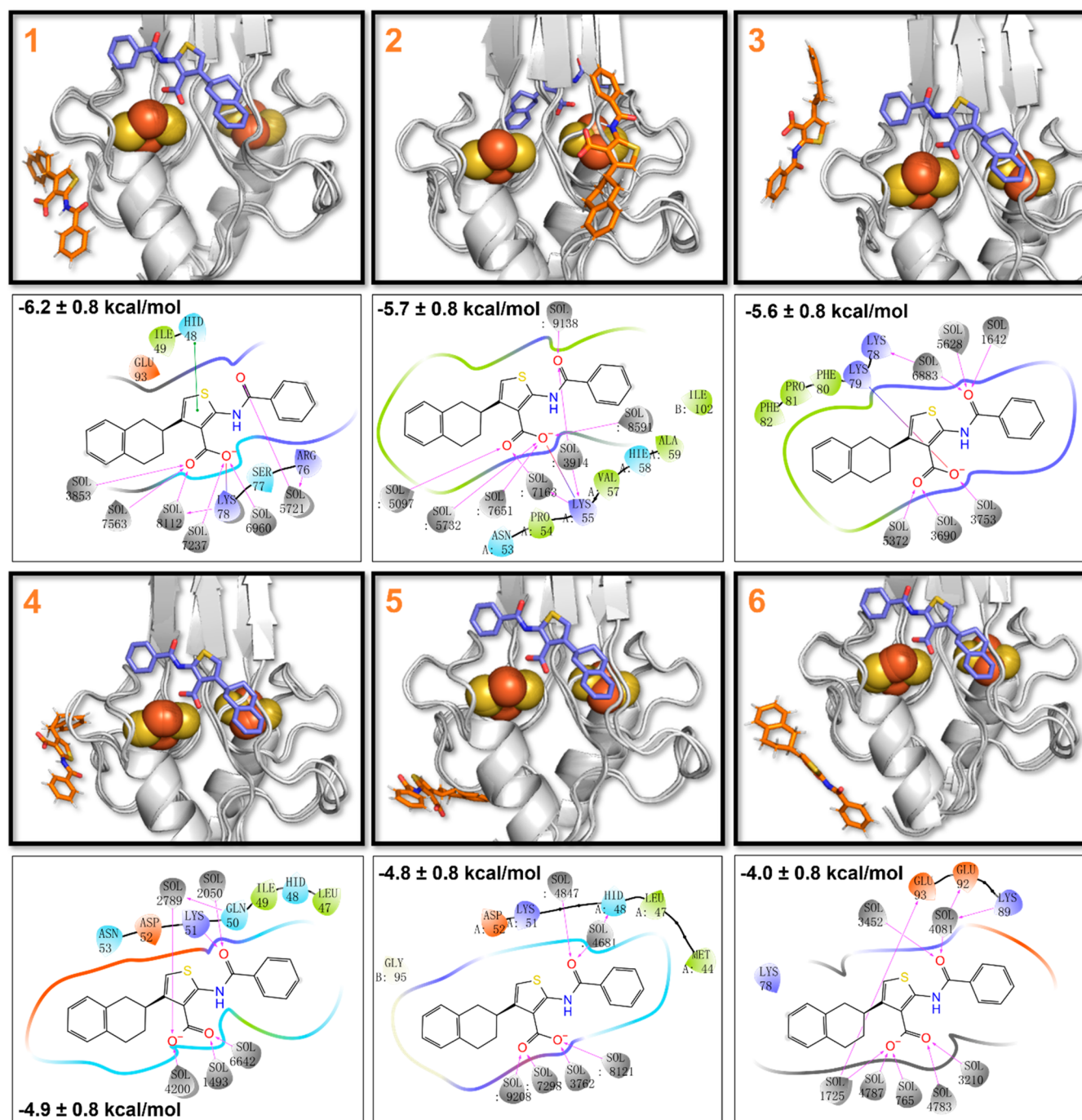


Figure 7. The ligand/protein interactions in II at 310 K. The crystal binding pose is shown in the slate stick as a reference, while the representative binding poses are shown in orange.

found at 293 K. The minima 1 and 2 are associated with the binding free energy of -8.2 ± 0.8 kcal/mol and -6.6 ± 0.8 kcal/mol, respectively.

In minimum 1, the tetralin group forms a π -cation interaction with Lys51 and hydrophobic interactions with Met44 and Leu47. Additionally, A's carbonyl oxygen includes an H-bond between His48, while the carboxylate group forms H-bonds with water molecules (Figure 6A, Table S5 in the SI). In minimum 2, the tetralin group forms a π - π stacking with Phe82 and hydrophobic interactions with Leu65, Ala69, and Val70. Its thiophene ring and amide moiety form polar van der Waals (vdW) interactions with Lys78 and Lys79. Besides,

carbonyl and carboxylate oxygens form H-bonds with water molecules (Figure 6B, Table S5 in the SI). For the sake of simplicity, we do not discuss the interactions with water, which are displayed in Figure 6A and 6B.

We next evaluated the impact of the protonation of His87 and/or cluster reduction on the free energy landscape. First, let us discuss the effect of the protonation of His87, *i.e.*, imidazole instead of imidazolate (complex II). The free energy landscape becomes much more complex, with as many as six minima, five of which (minimum 1, 3–6) are not too dissimilar in geometry to those of I at 293 K (Figure 3). In minimum 1 (-6.2 ± 0.8 kcal/mol, Tables 3 and S6 in the SI), the thiophene ring of A

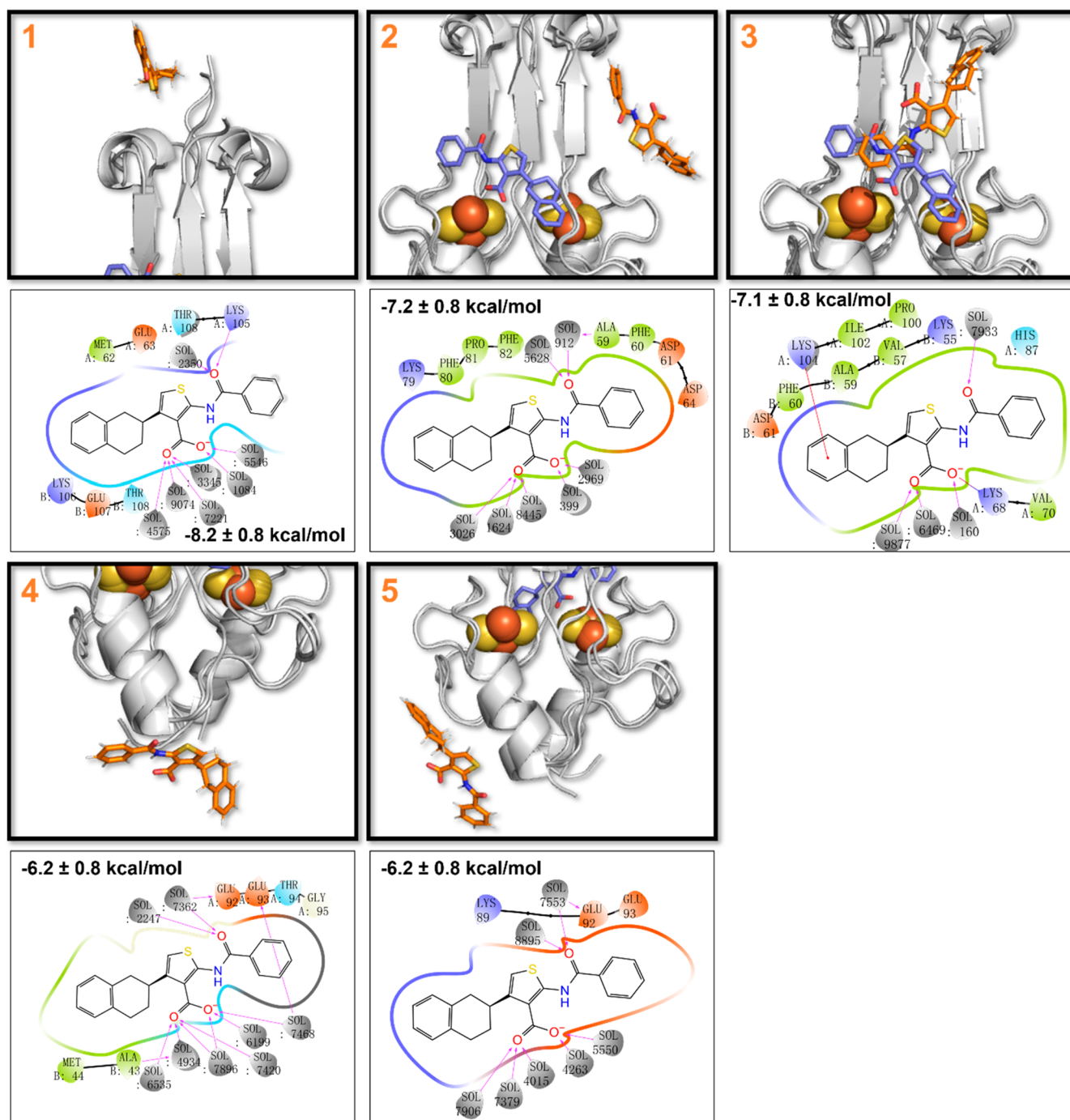


Figure 8. The ligand/protein interactions of A bound to III at 310 K. The crystal binding pose is shown in the slate stick as a reference, while the representative binding poses are shown in orange.

forms π - π stacking interactions with His48, hydrophobic interactions with Ile49, and interactions with the Ser77 backbone unit; A's carbonyl oxygen forms a water-mediated H-bond with Arg76; and the carboxylate group forms a salt bridge with Lys78 and H-bonds with solvent molecules; at times, its phenyl group forms an interaction with Glu93.

In the next minimum (2, -5.7 ± 0.8 kcal/mol), the tetralin group forms hydrophobic interactions with Pro54, while the phenyl ring interacts with Val57-Ala59 and Ile102; the thiophene ring interacts with Asn53; and the carboxylate oxygens form a salt bridge with Lys55 and H-bonds with water molecules (Figure 7).

In minimum 3 (-5.6 ± 0.8 kcal/mol), the tetralin and thiophene rings form hydrophobic interactions with Phe80-Phe82; the carboxylate forms a salt bridge with Ly79; and the carbonyl oxygen forms a water-mediated H-bond with Lys78.

The next poses are not significantly populated. In minimum 4 (-4.9 ± 0.8 kcal/mol), A's tetralin group forms metastable interactions with Asp52 and Asn53; the thiophene ring forms polar interactions with Gln50; and the phenyl ring forms hydrophobic interactions with Leu47 and Ile49 and, at times, with His48; in addition, the carbonyl oxygen forms an H-bond with Lys51.

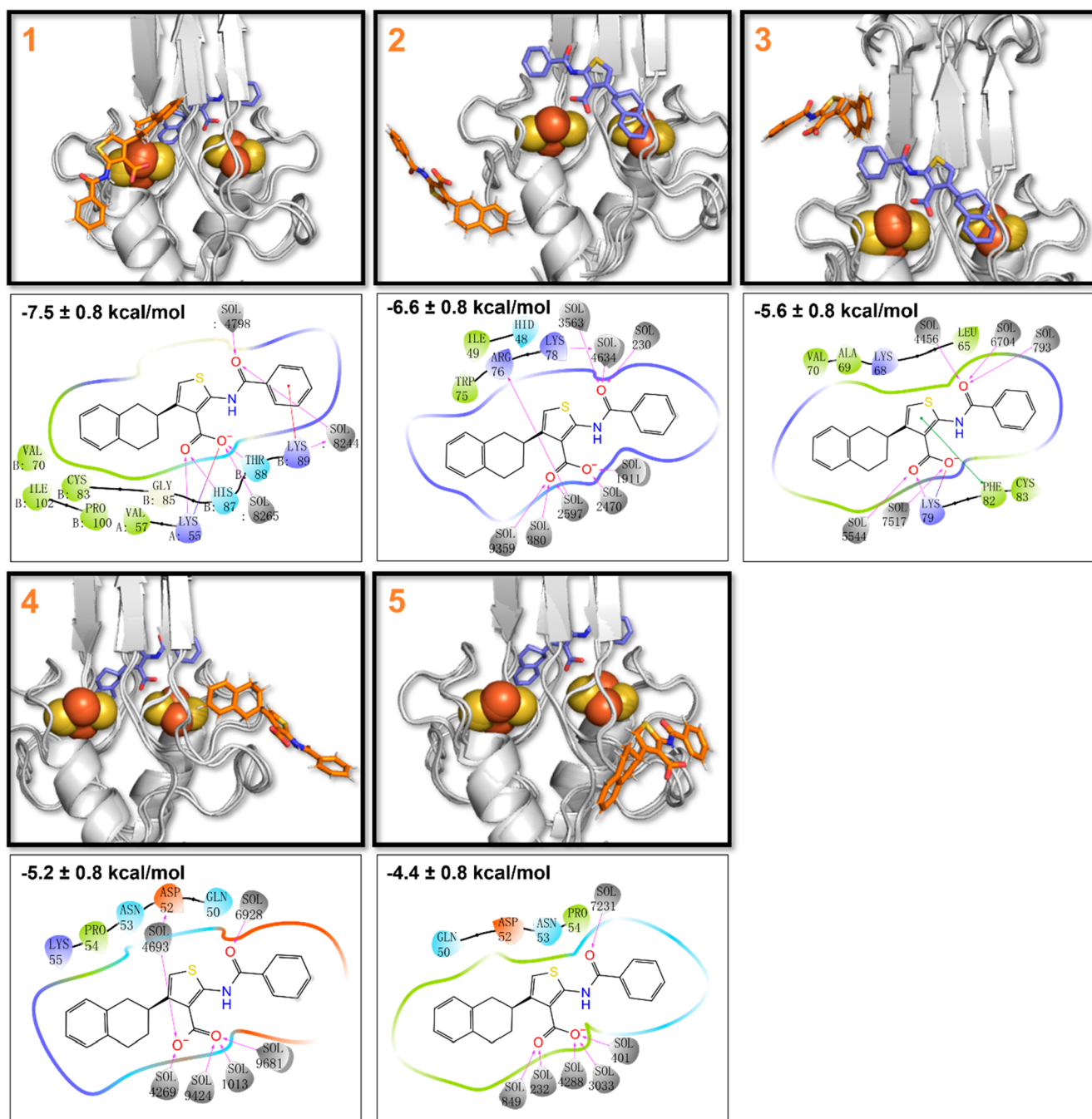


Figure 9. The ligand/protein interactions of **A** bound to **IV** at 310 K. The crystal binding pose is shown in the slate stick as a reference, while the representative binding poses are shown in orange.

In minimum 5 (-4.8 ± 0.8 kcal/mol) [As minimum 4 for **I** at 293 K, the poses of minima 5 and 6 are expected to be affected by the presence of the transmembrane domain of mNT absent in the model.], the tetralin group interacts with Gly95 and Met44, and the thiophene ring interacts with Lys51 and Asp52. Besides, the phenyl ring forms hydrophobic interactions with Leu47 and metastable interactions with His48, and the oxygen atoms of **A** form H-bonds with solvent molecules.

In minimum 6 (-4.0 ± 0.8 kcal/mol), the tetralin group forms metastable interactions with Lys78, while the benzene ring forms interactions with Glu92 and Glu93; the thiophene

ring forms interactions with Lys89; and its carboxylate and carbonyl oxygens form H-bonds with water molecules.

We finally focus on the effect of reduction (**III** and **IV** in Table 1). In the deprotonated form (**III**), the lowest binding free energy is similar to that of **I** (-8.2 ± 0.8 kcal/mol, Table 3), and the free energy landscape features five minima (Figure 8 and Table S7 in the SI).

In minimum 1, the ligand binds at the L2 loop of the β -cap (Figure 8). Specifically, the tetralin group forms polar metastable interactions with Glu63, Lys106, Glu107, and Thr108; its thiophene ring interacts with Met62 and Thr108 of another chain; and carbonyl oxygen forms an H-bond with

Lys106 of another chain. The ligand is instead found bound to L1 and L3 loops in minima 2, 4, and 5.

In minimum 2 (-7.2 ± 0.8 kcal/mol), the tetralin group of A forms hydrophobic interactions with Phe80 and Phe82 as well as, at times, interactions with Lys79; the thiophene ring forms interactions with Pro81, while the benzene ring interacts with Ala59 and Phe60 as well as, at times, Asp61 and Asp64.

A binds to the β -sheets in minimum 3 (-7.1 ± 0.8 kcal/mol); the tetralin moiety forms π -cation interactions with Lys104, hydrophobic interactions with Ala59, and metastable interactions with Asp61 and the main chain of Phe60; the thiophene ring forms hydrophobic interactions with Val57 and Ile102; the carboxylate oxygens form a salt bridge with Lys68; and the phenyl moiety forms hydrophobic interactions with Val70, Pro100, and, at times, with His87.

In minimum 4 (5) (both -6.2 ± 0.8 kcal/mol) [As in the previous cases, the two poses will be affected by the transmembrane domain absent in the calculations.], the tetralin forms hydrophobic interactions with Ala43 and Met44 (It interacts, at times, with Lys89.); the thiophene ring forms interactions with Thr94 and Gly95 (with Glu92 and Glu93); and the benzene ring, at times, interacts with the main chain of Glu92 and Glu93.

Protonation of the Fe-bound histidine (complex IV in Figure 9, Table S8 in the SI), decreases the lowest binding free energy (Table 3). Here, the ligand binds to the [2Fe–2S] cluster region and to the L1/L3 loops. In minimum 1 (-7.5 ± 0.8 kcal/mol), the tetralin group forms hydrophobic interactions with Val57, Val70, Cys83, Pro100, and Ile102; the thiophene ring interacts with Gly85; the phenyl ring forms a π -cation interaction with Lys89; and the carboxylate moiety forms a salt bridge with Lys55, along with H-bonds with His87 and Thr88.

In minimum 2 (-6.6 ± 0.8 kcal/mol), the tetralin group interacts, at times, with His48, Arg76, and Trp75; and the carbonyl oxygen forms an H-bond with three water molecules in which one also forms H-bonds with Lys78.

In minimum 3 (-5.6 ± 0.8 kcal/mol), the tetralin group forms hydrophobic interactions with Ala69, Val70, and Cys83 and metastable interactions with Lys68; the thiophene ring forms a π - π stacking with Phe82 and polar vdW interactions with the main chain of Leu65; and the carboxylate oxygen forms a salt bridge with Lys79.

In minimum 4 (-5.2 ± 0.8 kcal/mol), the tetralin moiety forms hydrophobic interactions with Pro54. It interacts, at times, with Asn53 and the main chain of Lys55; the thiophene ring interacts with Gln50 and Asp52.

In minimum 5 (-4.4 ± 0.8 kcal/mol), A binds with the L1 loop. Its thiophene ring forms hydrophobic interactions with Pro54; the benzene ring forms polar vdW interactions with Gln50 and Asn53 and a metastable interaction with Asp52.

4. CONCLUSIONS

We have presented a metadynamics study on the binding poses and affinity of ligand A to human mNT in an aqueous solution. Different protonation states of the iron bound His87 and redox states (see Table 1) were considered.

Our affinity is consistent with experiment in the same conditions. The simulations at the same temperature as those used for the X-ray structure of ref 11 further suggested that crystal packing likely stabilizes the pose of the ligand in the cluster region at the same temperature. Indeed, in an aqueous solution, where such packing forces are absent, A binds not

only to the [2Fe–2S] cluster binding region but also to the L1/L3 loops and L2 loops of the β -cap with multiple binding poses. One of the low energy poses shares a similarity with that of the X-ray structure. Here, the binding affinity of A fairly correlates to the intermolecular contacts formed by the ligand with the protein. When A binds to β -sheets and the [2Fe–2S] cluster binding region, it forms many contacts and has a high affinity with its target protein. *Vice versa*, when it binds to L1 and L3 loops, it does so with both low affinity and less intermolecular contacts to the target but more with the water molecules compared to the β -sheets and the [2Fe–2S] cluster region. In the X-ray structure, the ligand forms a much higher number of contacts, because it binds not only to the protein but also to its images. So, we may expect a different binding pose, as suggested by our calculations.

At physiological temperature, the redox and protonation states affect the free energy landscape in a highly nontrivial manner. In particular, the reduction on the [2Fe–2S] clusters of mNT with deprotonated His87 allows A to reach the L2 loop. The protonation of iron bound His87 on oxidized mNT leads to binding to the β 1 sheet and L1 loop. The reduction has little effect on the affinity.

Of course, the predicting power of our calculations depends crucially on the quality of the force field, which is challenged in multinuclear open shell systems such as Fe–S proteins. Experimental validation (such as NMR⁴⁴) would be of great help to establish the accuracy of our predictions. We would like nevertheless to close with a positive note, as the calculations here have provided the first picture of a ligand bound to the human mNT surface in an aqueous solution. This work may greatly help rational drug design of ligands targeting this protein, as it offers, for the first time, a complete and complex picture of ligands binding to one of the NEET proteins in a solution.

■ ASSOCIATED CONTENT

Data Availability Statement

ChemBio3D Ultra 12.0, Chem3D 16.0 (<http://www.cambridgesoft.com/>), and Gaussian 09 (<https://gaussian.com/>) software packages were used for ligand modeling. The program Glide was used for the ligand/protein docking (<https://www.schrodinger.com/products/gleide>). The software used here for MD and volume-based metadynamics is freely available. It consists of GROMACS (<https://www.gromacs.org/>) and of PLUMED (<https://www.plumed.org/>). All the data produced by this research is available upon request.

■ Supporting Information

The Supporting Information is available free of charge at <https://pubs.acs.org/doi/10.1021/acs.jcim.2c01280>.

Details on settings of molecular docking; force field and parameters of ligand A; convergence of MD simulations and metadynamics of A-mNT; ligand/protein interactions for I–IV complexes (PDF)

■ AUTHOR INFORMATION

Corresponding Author

Paolo Carloni – Department of Physics, RWTH Aachen University, 52074 Aachen, Germany; Computational Biomedicine, Institute of Advanced Simulation IAS-5 and Institute of Neuroscience and Medicine INM-9 and JARA Institute: Molecular Neuroscience and Imaging, Institute of Neuroscience and Medicine INM-11, Forschungszentrum

Jülich GmbH, 52425 Jülich, Germany; orcid.org/0000-0002-9010-0149; Email: p.carloni@fz-juelich.de

Authors

Ke Zuo – The Alexander Silberman Institute of Life Science, The Hebrew University of Jerusalem, 91904 Jerusalem, Israel; Department of Physics, RWTH Aachen University, 52074 Aachen, Germany; Computational Biomedicine, Institute of Advanced Simulation IAS-5 and Institute of Neuroscience and Medicine INM-9, Forschungszentrum Jülich GmbH, 52425 Jülich, Germany; Department of Physics, Università di Ferrara, 44121 Ferrara, Italy

Riccardo Capelli – Department of Biosciences, Università degli Studi di Milano, 20133 Milan, Italy; orcid.org/0000-0001-9522-3132

Giulia Rossetti – Computational Biomedicine, Institute of Advanced Simulation IAS-5 and Institute of Neuroscience and Medicine INM-9 and Jülich Supercomputing Center (JSC), Forschungszentrum Jülich GmbH, 52425 Jülich, Germany; Department of Neurology, Faculty of Medicine, RWTH Aachen University, 52074 Aachen, Germany; orcid.org/0000-0002-2032-4630

Rachel Nechushtai – The Alexander Silberman Institute of Life Science, The Hebrew University of Jerusalem, 91904 Jerusalem, Israel; orcid.org/0000-0002-3219-954X

Complete contact information is available at:
<https://pubs.acs.org/10.1021/acs.jcim.2c01280>

Author Contributions

K.Z. performed the calculations and data analysis. R.C., G.R., R.N., and P.C. supervised the project and wrote the paper with input from all authors.

Funding

K.Z. is supported by the Marie Skłodowska-Curie grant agreement No. 765048.

Notes

The authors declare no competing financial interest.

ACKNOWLEDGMENTS

We acknowledge the computing time granted by RWTH Compute Cluster (No. 3497 and No. 20134).

ABBREVIATIONS

mNT, mitoNEET; A, 2-benzamido-4-(1,2,3,4-tetrahydronaphthalen-2-yl)-thiophene-3-carboxylate; RMS, root mean squared; MD, molecular dynamics; PME, particle mesh Ewald; MetaD, metadynamics; CVs, collective variables; FES, free energy surface

REFERENCES

- (1) Paddock, M. L.; Wiley, S. E.; Axelrod, H. L.; Cohen, A. E.; Roy, M.; Abresch, E. C.; Capraro, D.; Murphy, A. N.; Nechushtai, R.; Dixon, J. E.; Jennings, P. A. MitoNEET is a uniquely folded 2Fe-2S outer mitochondrial membrane protein stabilized by pioglitazone. *P Natl. Acad. Sci. USA* **2007**, *104*, 14342–14347.
- (2) Lin, J. Z.; Zhou, T.; Ye, K. Q.; Wang, J. F. Crystal structure of human mitoNEET reveals distinct groups of iron-sulfur proteins. *P Natl. Acad. Sci. USA* **2007**, *104*, 14640–14645.
- (3) Hou, X. W.; Liu, R. J.; Ross, S.; Smart, E. J.; Zhu, H. N.; Gong, W. M. Crystallographic studies of human MitoNEET. *J. Biol. Chem.* **2007**, *282*, 33242–33246.
- (4) Nechushtai, R.; Karmi, O.; Zuo, K.; Marjault, H. B.; Darash-Yahana, M.; Sohn, Y. S.; King, S. D.; Zandalinas, S. I.; Carloni, P.;

Mittler, R. The balancing act of NEET proteins: Iron, ROS, calcium and metabolism. *Biochim Biophys Acta Mol. Cell Res.* **2020**, 1867, 118805.

(5) Marjault, H. B.; Zuo, K.; Mittler, R.; Carloni, P.; Nechushtai, R. NEET proteins as novel drug targets for mitochondrial dysfunction. In *Clinical Bioenergetics*; Ostojic, S., Ed.; Academic Press: 2021; Chapter 477, pp 477–488, DOI: [10.1016/B978-0-12-819621-2.00021-8](https://doi.org/10.1016/B978-0-12-819621-2.00021-8).

(6) Dicus, M. M.; Conlan, A.; Nechushtai, R.; Jennings, P. A.; Paddock, M. L.; Britt, R. D.; Stoll, S. Binding of Histidine in the (Cys)(3)(His)(1)-Coordinated [2Fe-2S] Cluster of Human mitoNEET. *J. Am. Chem. Soc.* **2010**, *132*, 2037–2049.

(7) Zuo, K.; Marjault, H. B.; Bren, K. L.; Rossetti, G.; Nechushtai, R.; Carloni, P. The two redox states of the human NEET proteins' [2Fe-2S] clusters. *J. Biol. Inorg. Chem.* **2021**, *26*, 763–774.

(8) Geldenhuys, W. J.; Funk, M. O.; Barnes, K. F.; Carroll, R. T. Structure-based design of a thiazolidinedione which targets the mitochondrial protein mitoNEET. *Bioorg. Med. Chem. Lett.* **2010**, *20*, 819–823.

(9) Geldenhuys, W. J.; Long, T. E.; Saralkar, P.; Iwasaki, T.; Nunez, R. A. A.; Nair, R. R.; Konkole, M. E.; Menze, M. A.; Pinti, M. V.; Hollander, J. M.; Hazlehurst, L. A.; Robart, A. R. Crystal structure of the mitochondrial protein mitoNEET bound to a benze-sulfonide ligand. *Commun. Chem.* **2019**, *2*, 77.

(10) Geldenhuys, W. J.; Yonutas, H. M.; Morris, D. L.; Sullivan, P. G.; Darvesh, A. S.; Leeper, T. C. Identification of small molecules that bind to the mitochondrial protein mitoNEET. *Bioorg. Med. Chem. Lett.* **2016**, *26*, 5350–5353.

(11) Marjault, H. B.; Karmi, O.; Zuo, K.; Michaeli, D.; Eisenberg-Domovich, Y.; Rossetti, G.; de Chasse, B.; Vonderscher, J.; Cabantchik, I.; Carloni, P.; Mittler, R.; Livnah, O.; Meldrum, E.; Nechushtai, R. An anti-diabetic drug targets NEET (CISD) proteins through destabilization of their [2Fe-2S] clusters. *Communications Biology* **2022**, *5*, 437.

(12) Hoang, L. G.; Gossen, J.; Capelli, R.; Nguyen, T. T.; Sun, Z.; Zuo, K.; Schulz, J. B.; Rossetti, G.; Carloni, P. Multiple Poses and Thermodynamics of Ligands Targeting Protein Surfaces: The Case of Furosemide Binding to mitoNEET in Aqueous Solution. *Front Cell Dev Biol.* **2022**, *10*, 886568.

(13) Lucas, X.; Bauza, A.; Frontera, A.; Quinonero, D. A thorough anion- π interaction study in biomolecules: on the importance of cooperativity effects. *Chem. Sci.* **2016**, *7*, 1038–1050.

(14) Infield, D. T.; Rasouli, A.; Galles, G. D.; Chipot, C.; Tajkhorshid, E.; Ahern, C. A. Cation- π Interactions and their Functional Roles in Membrane Proteins. *J. Mol. Biol.* **2021**, *433*, 167035.

(15) Capelli, R.; Carloni, P.; Parrinello, M. Exhaustive Search of Ligand Binding Pathways via Volume-Based Metadynamics. *J. Phys. Chem. Lett.* **2019**, *10*, 3495–3499.

(16) Allinger, N. L. Conformational-Analysis.130. Mm2 - Hydrocarbon Force-Field Utilizing V1 and V2 Torsional Terms. *J. Am. Chem. Soc.* **1977**, *99*, 8127–8134.

(17) Petersson, G. A.; Bennett, A.; Tensfeldt, T. G.; Allaham, M. A.; Shirley, W. A.; Mantzaris, J. A Complete Basis Set Model Chemistry.1. The Total Energies of Closed-Shell Atoms and Hydrides of the 1st-Row Elements. *J. Chem. Phys.* **1988**, *89*, 2193–2218.

(18) Petersson, G. A.; Allaham, M. A. A Complete Basis Set Model Chemistry.2. Open-Shell Systems and the Total Energies of the 1st-Row Atoms. *J. Chem. Phys.* **1991**, *94*, 6081–6090.

(19) Frisch, M. J.; Trucks, G. W.; Schlegel, H. B.; Scuseria, G. E.; Robb, M. A.; Cheeseman, J. R.; Scalmani, G.; Barone, V.; Mennucci, B.; Petersson, G. A.; Nakatsuji, H.; Caricato, M.; Li, X.; Hratchian, H. P.; Izmaylov, A. F.; Bloino, J.; Zheng, G.; Sonnenberg, J. L.; Hada, M.; Ehara, M.; Toyota, K.; Fukuda, R.; Hasegawa, J.; Ishida, M.; Nakajima, T.; Honda, Y.; Kitao, O.; Nakai, H.; Vreven, T.; Montgomery, J. A., Jr.; Peralta, J. E.; Ogliaro, F.; Bearpark, M.; Heyd, J. J.; Brothers, E.; Kudin, K. N.; Staroverov, V. N.; Kobayashi, R.; Normand, J.; Raghavachari, K.; Rendell, A.; Burant, J. C.; Iyengar, S. S.; Tomasi, J.; Cossi, M.; Rega, N.; Millam, J. M.; Klene, M.; Knox,

J. E.; Cross, J. B.; Bakken, V.; Adamo, C.; Jaramillo, J.; Gomperts, R.; Stratmann, R. E.; Yazyev, O.; Austin, A. J.; Cammi, R.; Pomelli, C.; Ochterski, J. W.; Martin, R. L.; Morokuma, K.; Zakrzewski, V. G.; Voth, G. A.; Salvador, P.; Dannenberg, J. J.; Dapprich, S.; Daniels, A. D.; Farkas, O.; Foresman, J. B.; Ortiz, J. V.; Cioslowski, J.; Fox, D. J. *Gaussian 09 Rev. A.02*; Wallingford, CT, 2009.

(20) Jorgensen, W. L.; Maxwell, D. S.; TiradoRives, J. Development and testing of the OPLS all-atom force field on conformational energetics and properties of organic liquids. *J. Am. Chem. Soc.* **1996**, *118*, 11225–11236.

(21) Harder, E.; Damm, W.; Maple, J.; Wu, C. J.; Reboul, M.; Xiang, J. Y.; Wang, L. L.; Lupyan, D.; Dahlgren, M. K.; Knight, J. L.; Kaus, J. W.; Cerutti, D. S.; Krilov, G.; Jorgensen, W. L.; Abel, R.; Friesner, R. A. OPLS3: A Force Field Providing Broad Coverage of Drug-like Small Molecules and Proteins. *J. Chem. Theory Comput* **2016**, *12*, 281–296.

(22) Friesner, R. A.; Banks, J. L.; Murphy, R. B.; Halgren, T. A.; Klicic, J. J.; Mainz, D. T.; Repasky, M. P.; Knoll, E. H.; Shelley, M.; Perry, J. K.; Shaw, D. E.; Francis, P.; Shenkin, P. S. Glide: A new approach for rapid, accurate docking and scoring. 1. Method and assessment of docking accuracy. *J. Med. Chem.* **2004**, *47*, 1739–1749.

(23) Halgren, T. A.; Murphy, R. B.; Friesner, R. A.; Beard, H. S.; Frye, L. L.; Pollard, W. T.; Banks, J. L. Glide: A new approach for rapid, accurate docking and scoring. 2. Enrichment factors in database screening. *J. Med. Chem.* **2004**, *47*, 1750–1759.

(24) Pesce, L.; Calandrini, V.; Marjault, H. B.; Lipper, C. H.; Rossetti, G.; Mittler, R.; Jennings, P. A.; Bauer, A.; Nechushtai, R.; Carloni, P. Molecular Dynamics Simulations of the [2Fe-2S] Cluster-Binding Domain of NEET Proteins Reveal Key Molecular Determinants That Induce Their Cluster Transfer/Release. *J. Phys. Chem. B* **2017**, *121*, 10648–10656.

(25) Lindorff-Larsen, K.; Piana, S.; Palmo, K.; Maragakis, P.; Klepeis, J. L.; Dror, R. O.; Shaw, D. E. Improved side-chain torsion potentials for the Amber ff99SB protein force field. *Proteins* **2010**, *78*, 1950–1958.

(26) Sorin, E. J.; Pande, V. S. Exploring the helix-coil transition via all-atom equilibrium ensemble simulations. *Biophys. J.* **2005**, *88*, 2472–2493.

(27) Jorgensen, W. L.; Chandrasekhar, J.; Madura, J. D.; Impey, R. W.; Klein, M. L. Comparison of Simple Potential Functions for Simulating Liquid Water. *J. Chem. Phys.* **1983**, *79*, 926–935.

(28) Aqvist, J. Ion Water Interaction Potentials Derived from Free-Energy Perturbation Simulations. *J. Phys. Chem-Us* **1990**, *94*, 8021–8024.

(29) Wang, J. M.; Wolf, R. M.; Caldwell, J. W.; Kollman, P. A.; Case, D. A. Development and testing of a general amber force field. *J. Comput. Chem.* **2004**, *25*, 1157–1174.

(30) Jakalian, A.; Jack, D. B.; Bayly, C. I. Fast, efficient generation of high-quality atomic charges. AM1-BCC model: II. Parameterization and validation. *J. Comput. Chem.* **2002**, *23*, 1623–1641.

(31) Essmann, U.; Perera, L.; Berkowitz, M. L.; Darden, T.; Lee, H.; Pedersen, L. G. A Smooth Particle Mesh Ewald Method. *J. Chem. Phys.* **1995**, *103*, 8577–8593.

(32) Hess, B.; Bekker, H.; Berendsen, H. J. C.; Fraaije, J. G. E. M. LINCS: A linear constraint solver for molecular simulations. *J. Comput. Chem.* **1997**, *18*, 1463–1472.

(33) Nose, S. A Molecular-Dynamics Method for Simulations in the Canonical Ensemble. *Mol. Phys.* **1984**, *52*, 255–268.

(34) Hoover, W. G. Canonical Dynamics - Equilibrium Phase-Space Distributions. *Phys. Rev. A* **1985**, *31*, 1695–1697.

(35) Parrinello, M.; Rahman, A. Polymorphic Transitions in Single-Crystals - a New Molecular-Dynamics Method. *J. Appl. Phys.* **1981**, *52*, 7182–7190.

(36) Berendsen, H. J. C.; Vanderspoel, D.; Vandrunen, R. Gromacs - a Message-Passing Parallel Molecular-Dynamics Implementation. *Comput. Phys. Commun.* **1995**, *91*, 43–56.

(37) Abraham, M. J.; Murtola, T.; Schulz, R.; Páll, S.; Smith, J. C.; Hess, B.; Lindahl, E. GROMACS: High performance molecular

simulations through multi-level parallelism from laptops to super-computers. *SoftwareX* **2015**, *1-2*, 19–25.

(38) Capelli, R.; Bochicchio, A.; Piccini, G.; Casasnovas, R.; Carloni, P.; Parrinello, M. Chasing the Full Free Energy Landscape of Neuroreceptor/Ligand Unbinding by Metadynamics Simulations. *J. Chem. Theory Comput* **2019**, *15*, 3354–3361.

(39) Limongelli, V.; Bonomi, M.; Parrinello, M. Funnel metadynamics as accurate binding free-energy method. *Proc. Natl. Acad. Sci. U. S. A.* **2013**, *110*, 6358–6363.

(40) Allen, T. W.; Andersen, O.; Roux, B. Energetics of ion conduction through the gramicidin channel. *Biophys. J.* **2004**, *101*, 117.

(41) Tribello, G. A.; Bonomi, M.; Branduardi, D.; Camilloni, C.; Bussi, G. Plumed 2: New feathers for an old bird. *Computer Physics Communications* **2014**, *185*, 604–613.

(42) The PLUMED consortium. Promoting transparency and reproducibility in enhanced molecular simulations. *Nat Methods* **2019**, *16*, 670–673.

(43) Bochicchio, A.; Rossetti, G.; Tabarrini, O.; Krauss, S.; Carloni, P. Molecular View of Ligands Specificity for CAG Repeats in Anti-Huntington Therapy. *J. Chem. Theory Comput* **2015**, *11*, 4911–4922.

(44) Kranjc, A.; Bongarzone, S.; Rossetti, G.; Biarnes, X.; Cavalli, A.; Bolognesi, M. L.; Roberti, M.; Legname, G.; Carloni, P. Docking Ligands on Protein Surfaces: The Case Study of Prion Protein. *J. Chem. Theory Comput* **2009**, *5*, 2565–2573.

Recommended by ACS

Phosphorylation Regulation Mechanism of $\beta 2$ Integrin for the Binding of Filamin Revealed by Markov State Model

Xiaokun Hong, Hai-Feng Chen, *et al.*

JANUARY 06, 2023
JOURNAL OF CHEMICAL INFORMATION AND MODELING

READ 

Persistent Path-Spectral (PPS) Based Machine Learning for Protein-Ligand Binding Affinity Prediction

Ran Liu, Jie Wu, *et al.*

JANUARY 16, 2023
JOURNAL OF CHEMICAL INFORMATION AND MODELING

READ 

Identification of Enolase 1 as a Potential Target for *Magnaporthe oryzae*: Integrated Proteomic and Molecular Dynamics Simulation

Jie Gao, Lijie Guan, *et al.*

DECEMBER 29, 2022
JOURNAL OF CHEMICAL INFORMATION AND MODELING

READ 

Challenges in Protein QM/MM Simulations with Intra-Backbone Link Atoms

Alexander Zlobin, Andrey Golovin, *et al.*

JANUARY 12, 2023
JOURNAL OF CHEMICAL INFORMATION AND MODELING

READ 

Get More Suggestions >